Sensors and Actuators B 239 (2017) 1289–1299

Contents lists available at ScienceDirect

Sensors and Actuators B: Chemical

journal homepage: www.elsevier.com/locate/snb

Microfluidic impedimetric sensor for soil nitrate detection using graphene oxide and conductive nanofibers enabled sensing interface

Md. Azahar Ali[a], Huawei Jiang[a], Navreet K. Mahal[b], Robert J. Weber[a], Ratnesh Kumar[a], Michael J. Castellano[b], Liang Dong[a,*]

[a] Department of Electrical and Computer Engineering, Iowa State University, Ames, IA 50011 USA
[b] Department of Agronomy, Iowa State University, Ames, IA 50011 USA

ARTICLE INFO

Article history:
Received 14 May 2016
Received in revised form 20 August 2016
Accepted 17 September 2016
Available online 22 September 2016

Keywords:
Microfluidics
Graphene oxide
Nitrate sensor
Soil sensor

ABSTRACT

This paper reports on a microfluidic impedimetric nitrate sensor using a graphene oxide (GO) nanosheets and poly(3,4-ethylenedioxythiophene) nanofibers (PEDOT-NFs) enabled electrochemical sensing interface. The sensor has demonstrated the ability to accurately detect and quantify nitrate ions in real samples extracted from soil. The PEDOT NFs-GO composite serves as an effective matrix for immobilization of nitrate reductase enzyme molecules. The oxygenated functional groups available at GO allows an increased charge transfer resistance of the electrochemical electrode. Microscopic, spectroscopic, and electrochemical studies were systematically conducted to illustrate synergic interactions between the GO and PEDOT NFs. The sensor provides a sensitivity of 61.15 Ω/(mg/L)/cm^2 within a wide concentration range of 0.44–442 mg/L for nitrate ions in agricultural soils. The detection limit of the sensor is 0.135 mg/L with good specificity, reliability, and reproducibility.

© 2016 Elsevier B.V. All rights reserved.

1. Introduction

Nitrate (NO_3^-) is a critical nitrogen (N) source for plant growth [1,2], but is highly soluble in the soil solution and easily lost to the environment where it can degrade air and water quality. Indeed, the United States Environmental Protection Agency regulates NO_3^- concentration in drinking water at a maximum of 10 mg NO_3^--N/L (nitrogen in nitrate per liter) or 44.2 mg NO_3^-/L (nitrate per liter).[2] Soil nitrate has two major sources: microbial transformation of native soil organic nitrogen and exogenous N fertilizer inputs. In aerobic soils, heterotrophic microbes convert organic N to ammonium and chemoautotrophic microbes convert ammonium to nitrate *via* nitrification. Plants are able to absorb a variety of organic and inorganic N compounds, but in agricultural soils, nitrate is the major source of N uptake [1]. However, due to substantial losses from leaching to water and microbial denitrification, soil NO_3^- availability often limits crop production [2]. Currently, measurements of soil NO_3^- are used by farmers to avoid insufficient N fertilizer inputs that limit crop production and excessive N fertilizer inputs that decrease profitability and pollute the environment. But, these tests are relatively inaccurate because the soil must be manually sampled in the field and analyzed in a laboratory, which creates a 5–10 days delay between measurement and data availability. Rapid and accurate soil NO_3^- sensing could improve N fertilizer inputs, thereby increasing profitability and environment quality. Therefore, there is an urgent need to develop sensitive, miniature, and low cost nitrate sensors [3–8].

Electrochemical sensors often use biochemical receptors to recognize specific target molecules and produce electrical signals by catalytic reaction [9]. With high sensitivity, sign-to-noise ratio, and selectivity, they have played an important role for real-time measurements of biochemical species in many applications [9–13]. For nitrate detection, researchers have developed sensors using a variety of chemically modified electrodes based on the principle of electrocatalytic reduction of nitrate ions [3–7,14–19]. An electrochemical nitrate sensor has been developed using boron-doped diamond electrode modified with copper nanoparticles [18]. Another sensor based on copper nanostructures has also been developed for nitrate determination in foodstuffs and water [19]. State-of-the-art portable nitrate sensors include “NISE sc ISE Nitrate Probe” and “Neulog Nitrate Ion Selective Sensor” by Hach and Neulog, respectively. Both the sensors utilize potentiometric ion-selective measurements. These existing electrochemical sensors have led to significant improvement toward rapid and low-cost detection of nitrate ions. However, there is still much room for improvement of sensitivity, limit-of-detection (LOD), portabil-

* Corresponding author.
E-mail address: ldong@iastate.edu (L. Dong).

http://dx.doi.org/10.1016/j.snb.2016.09.101
0925-4005/© 2016 Elsevier B.V. All rights reserved.

ity, consumption of agent and reagent, and cost-effectiveness. In particular, as the critical element of electrochemical sensors, high-performance bioelectrodes require large electrochemical surface area, high loading capacity of receptors, high heterogeneous electron transfer rate, high affinity with target molecules, and easy fabrication.

Recently, poly(3,4-ethylenedioxythiophene) (PEDOT) has attracted much attention, due to its inherent stability, high conductivity, structural uniformity, and biocompatibility [20–23]. This material is considered as one of the most stable conducting polymers available at present. Because the undesired α, β- and β, β-couplings are not present within the polymer backbone, PEDOT has high electrical conductivity that ensures fast electron transfer [23,24]. In addition, the positively charged backbone of PEDOT allows for electrostatic binding with the negatively charged nanostructured materials or bio-species such as cells and enzymes [25]. PEDOT has been adopted in many biological and chemical sensors [26–28]. Recently, it has been shown that combining two-dimensional graphene oxide (GO) nanosheets with PEDOT could improve surface functionality of PEDOT, owing to the presence of the abundant functional groups at GO such as epoxide, hydroxyl, and carboxylic groups [29–36]. This has led to improved performances of electrocatalysts [35] and biosensors [36].

With recent advances in nanotechnology, functionalized one-dimensional (1D) conducting polymer nanostructures (CPNs), including nanofibers (NFs) [37,38], have offered favorable properties for chemical and biological sensors due to their large surface area, high conductivity, controllable composition, and fast electron transfer of a recognition event along their longitudinal axis [39,40]. In the past decade 1D CPNs have been investigated for use in many environmental monitoring and biomedical diagnostics applications [39,41]. In addition, PEDOT NFs have been developed using electrospinning, an inexpensive nanomanufacturing technique. In order to develop applications with PEDOT NFs for detecting biochemical molecules [39], several methods have been used to facilitate surface functionalization of PEDOT NFs, including using polystyrene [42,43], carboxylation by acid treatment [44], alkynes functionalization by click-reaction [44], microemulsion polymerization with acid [45], and perfluoro-functionalization by electro-polymerization [46].

In this paper, we report on the development of a microfluidic impedimetric sensor for detecting nitrate ions, using electrospun PEDOT NFs conjugated with both GO nanosheets and nitrate reductase (NiR) enzyme molecules as an electrochemical bioelectrode. The PEDOT NFs-GO composite is drop-coated on a gold (Au) electrode to form the working electrode (WE) of the microfluidic electrochemical sensor that integrates an Au counter electrode (CE) and a silver/silver chloride (Ag/AgCl) reference electrode (RE) inside a microfluidic channel (Fig. 1a). The functional groups (e.g., carboxyl and hydroxyl) of GO nanosheets facilitate immobilization of enzyme molecules on the surface of electrospun PEDOT NFs *via* EDC-NHS coupling chemistry for catalytic reaction with nitrate ions, and provide a high charge transfer resistance (R_{ct}) for the NiR/PEDOT NFs-GO composite based bioelectrode (Fig. 1b). Quantification of nitrate concentration in real samples extracted from soils is achieved on the sensor by an electrochemical impedance spectroscopy (EIS) method. High sensitivity of the sensor is obtained, due to a high electrochemical surface area and an improved heterogeneous electron rate of the composite. High selectivity of the sensor is realized by the enzyme molecules covalently anchored on the surface of GO nanosheets. By leveraging the excellent properties of the PEDOT NFs-GO composite with many benefits of microfluidics such as their portability, minimal amounts of samples and reagents, fast response time, and experimental parallelization, [47] the microfluidic sensor providesa promising sensor platform for the detection of nitrate ions in soils. To our knowledge, there is no report available on constructing a microfluidic nitrate sensor using the PEDOT NFs-GO composite with high sensitivity and specificity.

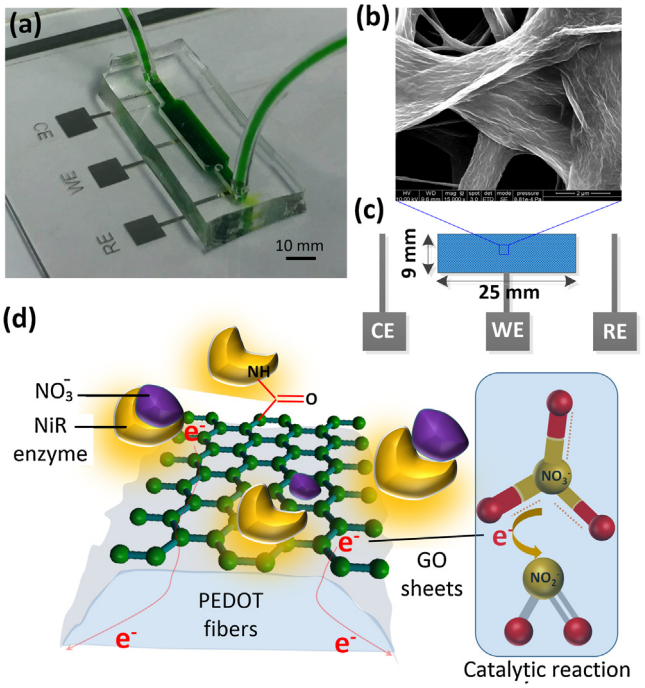

Fig. 1. (a) Photo of the fabricated microfludic sensor using a PEDOT NFs-GO composite to modifiy the working electrode for detection of nitrate ions. The channel was loaded with food dye for easy visualization. (b) Scanning electron microscopic (SEM) image for the PEDOT NFs-GO composite. (c) Geometry and layout of the working electrode of the sensor. (d) Schematic of the surface immobilization of PEDOT NFs-GO with NiR enzyme to realize electrochemical nitrate detection by catalytic conversion of nitrate to nitrite.

2. Experimental

2.1. Device fabrication

Details of fabricating a polydimethylsiloxane (PDMS) microfluidic channel, and Au and Ag/AgCl electrodes on a glass substrate are described in Supplementary information. Detail of chemicals and synthesis of PEDOT NFs by electrospinning [42] are also given in Supplementary information (Fig. S1).

Well-dispersed solution was prepared by mixing 0.4 mg of GO nanosheets and 1 mg of PEDOT NFs powders in 1 mL ethanol and sonicated for 2 h at room temperature (21 °C). Before deposition of the PEDOT NFs-GO composite, the Au electrode was treated with oxygen plasma to obtain a hydrophilic surface. 50 μL of the dispersed solution was spread onto the Au surface by drop casting. The treated Au electrode was then dried for 2 h in air at 40 °C. The surface of the PEDOT NFs could be strongly interact with the GO nanosheets due to π–π interactions [48] or electrostatic interactions (Fig. S2, Supplementary information). For control studies, the PEDOT NFs were also deposited on the surface of Au electrode without incorporating GO nanosheets.

NiR enzyme molecules were immobilized on the surface of PEDOT NFs-GO electrode *via* EDC—NHS chemistry. The −COOH groups at the GO surface allowed for covalent binding with $-NH_2$ groups of enzyme molecules by formation of C—N amide bond. 20 mL of a mixture of EDC and NHS at the volume ratio of 1:1 was dropped onto the PEDOT NFs-GO surface, where the EDC (0.2 M) acted as a coupling agent and NHS (0.05 M) as an activator. 10 μL of NiR solution (3.5 mg/mL) was dropped and spread onto the GO acti-

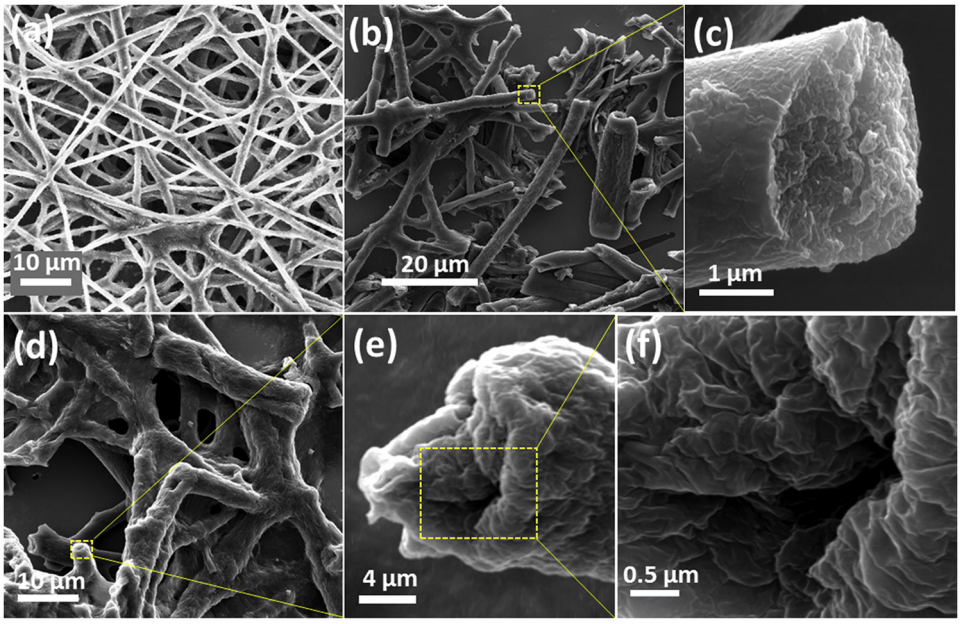

Fig. 2. SEM images of as-synthesized PEDOT NFs (a), dispersed PEDOT NFs deposited on the surface of Au electrode (b), tip of fragmented PEDOT NF (c), and GO nanosheets decorated PEDOT NFs (d–f).

vated surface and then kept for 12 h under a humid condition at 4 °C. To remove any unbound enzyme molecules from the electrode surface, the phosphate-buffered saline (PBS) solution was used to wash the electrode. This process allowed forming C—N bond between −COOH groups at GO and $-NH_2$ groups at NiR enzyme molecules as evident by the Fourier transform infrared spectroscopy (FT-IR) and X-ray photoelectron spectroscopy (XPS) analyses. After modifying the WE with the PEDOT NFs-GO composite and NiR enzyme molecules, the PDMS channel was treated by oxygen plasma and then bonded to the glass slide containing all the WE, CE and RE electrodes. Therefore, the microfluidic sensor was realized.

2.2. Extraction of analyte solutions from real soil sample and calibration of nitrate level

For the determination of nitrate levels, soil samples were collected from a *Zea mays* farm field with different intensities of artificial drainage (artificial drainage is common in *Z. mays* production fields). Soil moisture content of each sample was determined by weighing 10 g of field moist soil in an aluminum boat. Samples were dried at 105 °C until constant mass, and the gravemetric moisture content was calculated by mass of water per unit mass of dry soil (g/g) (Table S1, Supplementary information). To extract nitrate from each sample, 11–14 g of field moist soil was weighed in five specimen cups. 50 mL of 2 M KCl solution was added to each specimen cup and shaked on a reciprocal shaker for 1 h. After that, the solutions were filtered using Whatman #1 filter paper into 50 mL centrifuge tubes and the filtrates were kept frozen until analyzed.

To prepare test samples, 1000 mg/L of KNO_3 standard stock solution was prepared and diluted into eight different concentrations ranging from 0 to 44.2 mg/L of NO_3^-. 50 µL of each standard stock solution and soil extracts were pipetted into conventional 96-well microplate using an electronic pipette. Subsequently, 250 µL of reagent VCl_3/Griess-Ilosvay solution was added into each microplate well and kept at dark place for 24 h [49]. Using the PowerWaveX Select Scanning Microplate Spectrophotometer, the absorbance signals recorded at a fixed wavelength of 540 nm of monochromatic light. The absorbance signal increased with the increase in concentration of nitrate ions (Fig. S3a, Supplementary information). The linear relation of absorbance-concentration plot (standard curve) for known standards was determined: $y = 0.331x + 0.156$; $r^2 = 0.9951$ (Fig. S3b). Table S2 (Supplementary information) shows the concentrations of NO_3^- obtained from the extracted soil samples. One of these NO_3^- samples was diluted into different concentrations from 0.044 to 44.2 mg/L.

In order to perform measurements using the fabricated microfluidic device, the extracted sample solutions were loaded into a syringe (1 mL, BD Luer-Lok™) and infused into the device using a syringe pump (KDS 210, KD Scientific) through a needle and microfluidic tubing.

3. Results and discussion

3.1. Microscopic studies

Fig. 2a shows the SEM image of the as-synthesized PEDOT NFs. The NFs appeared in a mixed form of individuals and bundles of fibers. The soldered junctions of the fiber bundle were observed, presumably because of the strong electrostatic interaction between individual fibers [42]. Fig. 2b shows the PEDOT NFs deposited on the surface of oxygen plasma treated Au electrode. The as-synthesized PEDOT NFs were fragmented into short rods due to the sonication treatment prior to the deposition. The attachment between Au and PEDOT NFs occurred owing to the covalent interactions of the sulphur atoms present in the NFs with the Au substrate. Fig. 2c shows the individual fragmented PEDOT NF at a high magnification. The GO nanosheets coated on the PEDOT NFs are clearly seen in Fig. 2d. The close-up of the fiber tip (Fig. 2e and f) indicates the presence of GO wrinkles on the surface of PEDOT. The wrinkle formation may further facilitate the immobilization of the NiR enzyme molecules *via* the formation of C—N amide bond.

For TEM studies, the fragments of PEDOT NFs with GO nanosheets were dispersed in ethanol (≥99.5% purity) by sonication and then drop-casted onto holey carbon copper grids for imaging. Images in Fig. 3a and b show the overview of the dispersed PEDOT NFs and the soldering of PEDOT NFs. Fig. 3c shows an individual PEDOT NF with a core material, which presumably was PVP. The folding and wrinkles of GO nanosheets are shown on the surface of

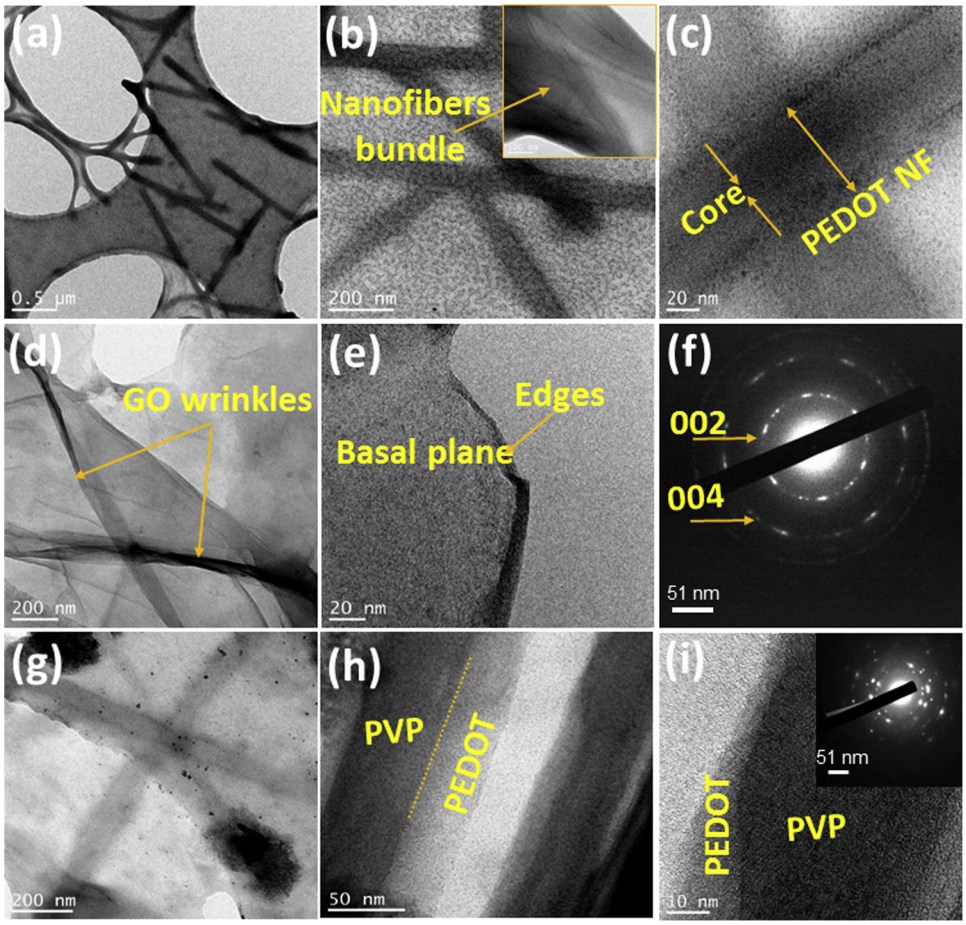

Fig. 3. TEM images of PEDOT NFs (a–c) and GO nanosheets (d–e). Inset of (b) shows a bundle of PEDOT NFs. Image (f) shows the SAED pattern of GO nanosheets. Images (g–i) show the PEDOT NFs coated with GO. Inset of (i) gives the SAED pattern of PEDOT NFs-GO composite.

holy carbon grid (Fig. 3d and e). The (002) and (004) planes of GO appeared in the selected area diffraction (SAED) pattern due to the crystalline structure of GO (Fig. 3e). The covering of GO nanosheets on the surface of PEDOT NFs is shown in Fig. 3g–i. Fig. 3h and i also depict the modification of GO nanosheets on the surface of PEDOT NFs, due to their electrostatic interactions. The appearance of more rings for the SAED pattern of GO sheets with PEDOT NFs (inset of Fig. 3i) indicates the strong GO attachment to the PEDOT NFs.

3.2. Spectroscopic studies

Spectroscopic studies were carried out to confirm the formation of PEDOT NFs-GO composite and the immobilization of NiR enzyme on the surface of the composite by quantifying important functional groups such as C—O, C—C, and C=C, —COOH present in the composite.

For quantitative confirmation of surface functionalization, we conducted elemental analyses using energy-dispersive X-ray (EDX) spectra for the PEDOT NFs and PEDOT NFs-GO before and after the NiR enzyme immobilization (Fig. S4 in Supplementary information). The C and O elements increased by ~40% and ~50%, respectively, after the immobilization. This can confirm the efficient incorporation of enzyme molecules. More details of EDX studies are given in the Supplementary information.

Raman spectroscopy measurements were conducted for the PEDOT NFs-GO composite (Fig. S5a in Supplementary information). The Raman spectrum of PEDOT NFs exhibited three peaks at 996, 1139, 1202 and 1363.8 cm^{-1}, due to oxyethylene ring deformation, C—O stretching, C—C inter-ring, and C—C stretching, respectively, in plane modes. The dominant peaks at 1447 and 1505 cm^{-1} were assigned to C=C stretching in plane modes (antisym.) and C=C stretching in plane modes (sym.), respectively. The peaks at 1590 and 1641 cm^{-1} corresponded to quinoid structure and thiophene ring vibration of NFs, respectively. In the case of GO, the peaks at 1350 cm^{-1} and 1603 cm^{-1} corresponded to disorder (D) and graphitic (G) modes, respectively. The atomic layer of GO was calculated to be 0.632 nm, indicating that there were about two layers of GO nanosheets (Eq. S1 in Supplementary information). The peaks at 1350 cm^{-1}, 1447 and 1505 cm^{-1} in the spectrum of PEDOT NFs remained unshifted even with the incorporation of GO nanosheets. The peak at 1587 cm^{-1} may be caused by overlapping between graphitic (1603 cm^{-1}) and quinoidal structure (1590 cm^{-1}) peaks.

FT-IR spectroscopy measurements were conducted for the PEDOT NFs before and after the incorporation of GO nanosheets and NiR enzyme molecules to further confirm the surface functionalization of GO and covalent interaction of NiR with PEDOT NFs (Fig. S5b–d in Supplementary information). In the PEDOT NFs (Fig. S5b in Supplementary information), the peaks at 1380–1521 cm^{-1} corresponded to C—C and C=C stretching of quinoidal structure and ring stretching of thiophene ring. After the GO modification, the functional groups such as C—OH, C—O—C, and —COOH at the PEDOT NFs-GO composite appeared. The peak at 1250 cm^{-1} corresponded to amide III, and the peak in the range of 1440–1640 cm^{-1} was assigned to the amide I indicating the enzyme immobilization [50]. Detailed explaination of the FT-IR measurement results is provided in Supplementary information.

XPS measurements were conducted to quantify various functional groups present at the PEDOT NFs, PEDOT NFs-GO, and

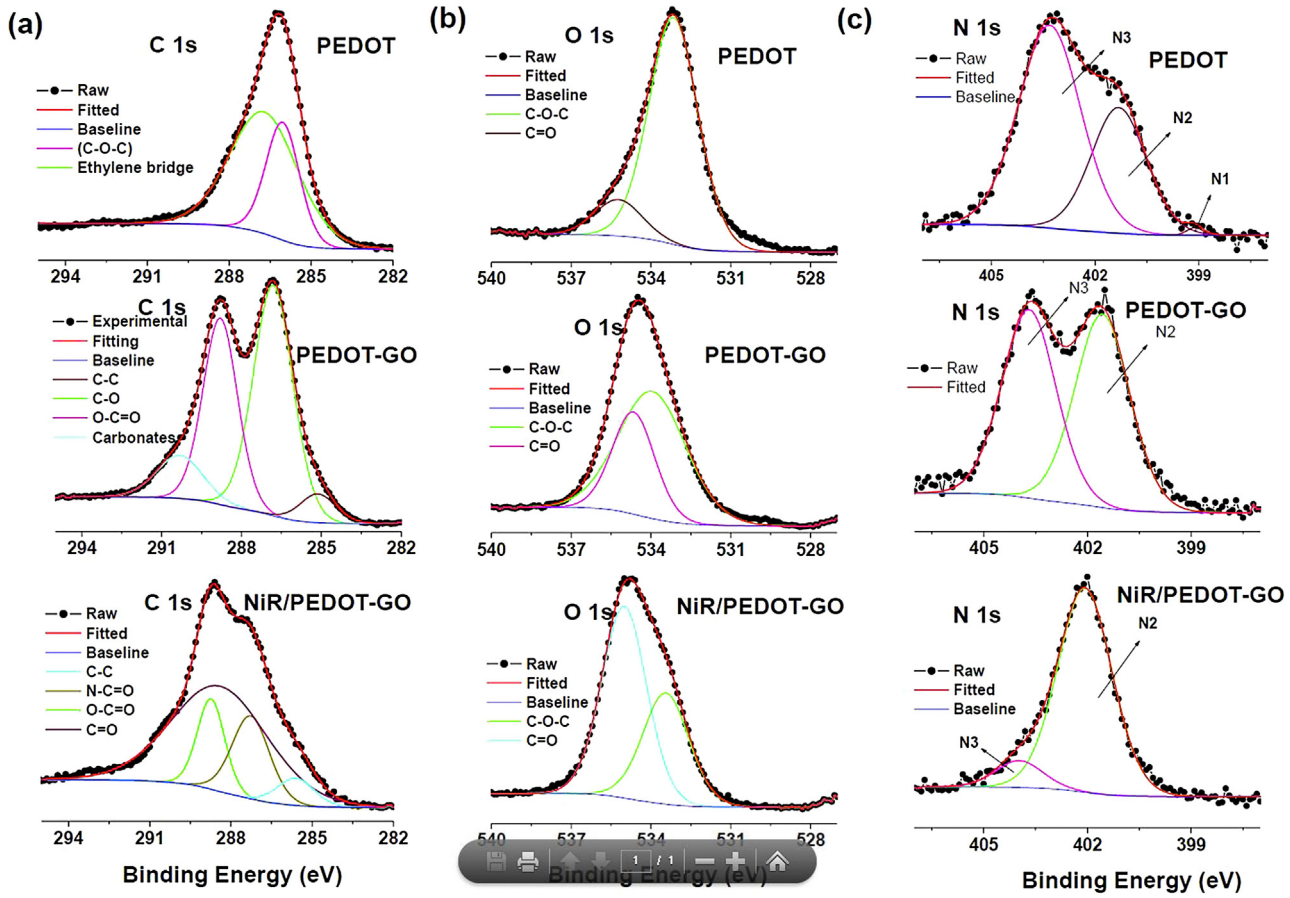

Fig. 4. XPS spectra for C 1s (a), O 1s (b) and N 1s (c) for PEDOT NFs, PEDOT NFs-GO and NiR/PEDOT NFs-GO films, respectively, with high-resolution deconvoluted peaks.

NiR/PEDOT NFs-GO. Fig. S6a (Supplementary information) shows the wide-scan spectra for the PEDOT NFs, PEDOT NFs-GO, and NiR/PEDOT NFs-GO. After the deconvolution of S 2p, three peaks were found at 165.5 eV, 169.3 eV, and 170.6 eV, corresponding to neutral S (S1), cationic S^+ (S2) associated with the PEDOT backbone, and highly oxidized sulfonate group (S3), respectively. [51,52] Due to the strong affinity of sulphur atom with Au, the neutral sulphur species was bound with the Au surface *via* covalent interactions. The presence of sulfonate groups and cationic S^+ indicates that the PEDOT NFs were positively charged (Fig. S6b–c, Supplementary information). Thus, the negatively charged GO nanosheets could interact with the PEDOT NFs *via* electrostatic interactions [53]. Due to the iron residues from FeTos during polymerizing EDOT, two peaks were observed at 72 and 725 eV owing to Fe 2p3 and 2p1 (Fig. S6d, Supplementary information). The peak for C 1s core-level spectrum of PEDOT NFs was deconvoluted into two components at 286.7 and 286.7 eV assigned to O—C—O (at.%:) in the β position and C—O—C in the ethylene bridge of NFs (Fig. 4a) [54]. After the GO incorporation, the characteristic peak for C1s was split into four peaks at 285.1, 286.8, 288.7 and 290.3 eV corresponding to C-S or graphitic C—C, epoxy C—O—C, carboxylic O—C=O (atomic concentration: 35.1%) and carbonates, respectively, of GO nanosheets. After the NiR immobilization, an additional peak in C 1s core-level spectrum was found at 287.2 eV with a full-width half maxima (FWHM) of 1.62 assigned to amide bond (N—C=O). Table S3 shows the binding energies, FWHM, and corresponding atomic concentrations of deconvoluted peaks obtained from C 1s, O 1s and N 1s. In EDC-NHS chemistry, the amide bond was formed by the covalent interaction of a carboxylic acid at GO nanosheet and an amine at NiR enzyme molecule, gaining one amide bond by losing one O—C=O. Thus, the atomic concentration of O—C=O in PEDOT NFs-GO reduced to 20.3% after the NiR immobilization. This indicates that the O—C=O groups play a role in forming amide bond on the surface of electrode. In the core-level spectrum of O 1s (Fig. 4b, PEDOT NFs), two peaks at 533.1 and 535.2 eV corresponded to epoxy (C—O—C) and carbonyl (C=O) functional groups, respectively. The binding energies of these peaks found in PEDOT NFs were slightly shifted with the incorporation of GO nanosheets; however, the atomic concentration increased to 18.5%, and after the NiR treatment it increased to 32.5% further. The peaks of N 1s region in PEDOT were located at 399.1, 401.3 and 403.3 eV, revealing uncharged deprotonated imine (N1; —C=N—), nitrogen moieties (N2; —NH—), and protonated and hydrogen bonded amine (N3; —NH^+—), respectively, due to the utilization of pyridine and polyvinylpyrrolidone during the synthesis of PEDOT NFs (Fig. 4c) [55]. With the GO modification, the spectrum of PEDOT NFs exhibited two peaks, i.e., N2 and N3, with higher binding energies. After the NiR immobilization, the peak at 402.0 eV with an enhanced atomic concentration (89.8%) may be due to the formation of amide (N—C=O) bond [56].

3.3. Electrochemical characterization

Cyclic voltammetry (CV) measurements (Fig. 5a) were conducted to study the interfacial properties and redox activity of the sensors using different electrodes, including PEDOT NFs, PEDOT NFs-GO, and NiR/PEDOT NFs-GO composites. Their electrochemical peak current (I_p), peak-to-peak separation potential (ΔE), diffusion coefficient (D), surface concentration (Γ), electrochemical active surface area (A_{el}), and heterogeneous electron transfer rate (k_s)

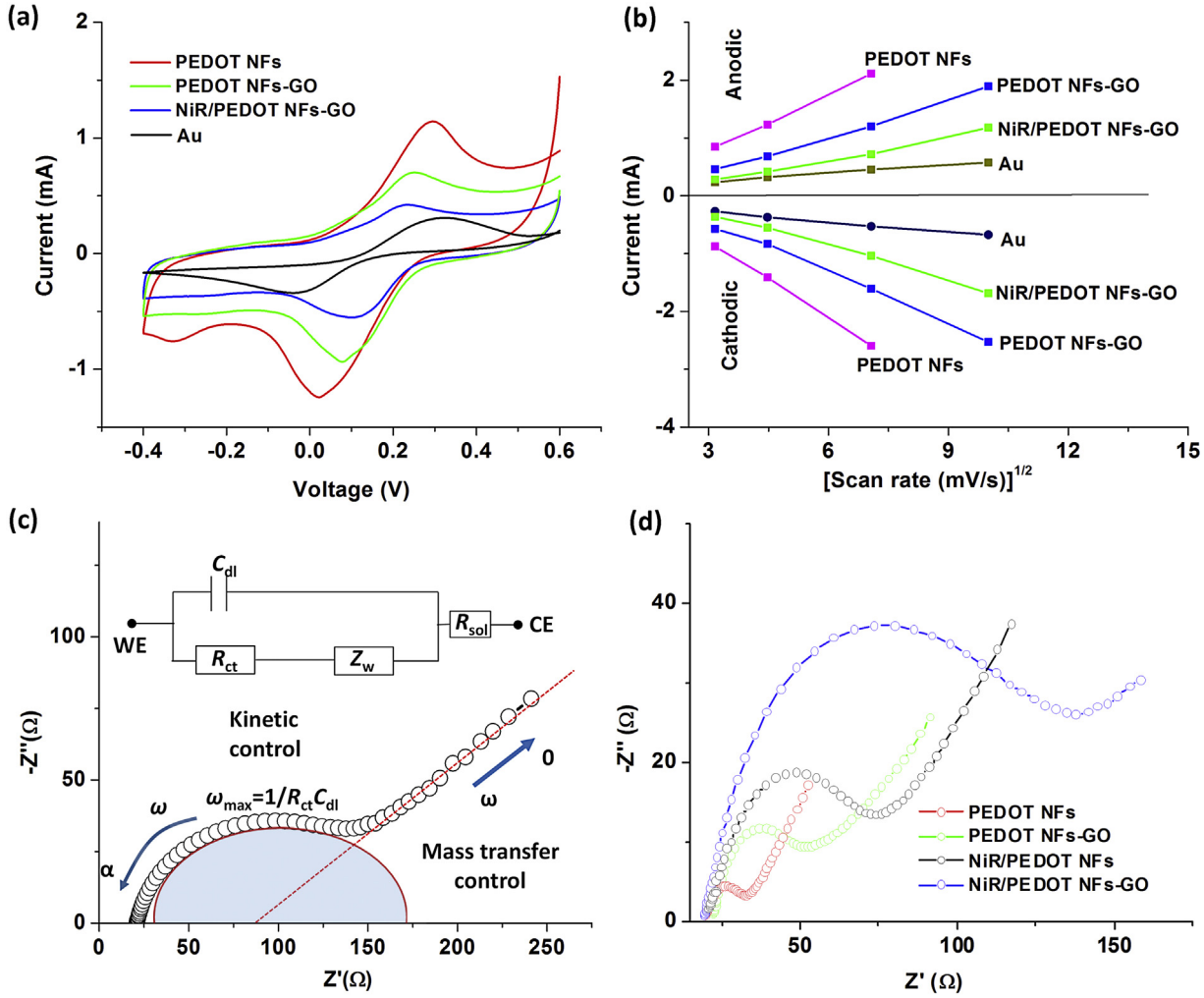

Fig. 5. (a) CV studies for different electrodes at a scan rate of 20 mV/s in 50 mM PBS (0.9% NaCl; pH: 7.0) using 5 mM $K_3[Fe(CN)_6]^{3-/4-}$ as a redox mediator. (b) Anodic and cathodic peak current variations as a function of square root of scan rate for different electrodes. (c) Nyquist plot and corresponding fitting for Au electrode by EIS method for calculating R_{ct} and C_{dl} values. The semicircle and straight regions indicated kinetic and mass transfer control. Inset shows the equivalent circuit model for EIS spectra. The amplitude was set to 1 mV, the bias potential was at 1 mV, and the frequency range was set to 1.0 Hz to 100×10^3 Hz. (d) EIS spectra for PEDOT NFs and PEDOT NFs-GO electrodes before and after NiR immobilization.

were calculated using Eq. S2–S9 (Supplementary information) and summarized in Table 1. Compared to the bare Au electrode, the PEDOT NFs had a higher electrochemical peak current of 1.13 mA on the order of a 3-time increase and a lower peak-to-peak separation voltage because of an enhanced electron transfer rate. The PEDOT NFs exhibited a higher conductivity due to the absence of α, β- and β, β-couplings within the polymer backbone [23,24]. After the GO incorporation, the electrochemical surface area of the PEDOT NFs-GO became larger; but, both the redox activity and peak current reduced, which may be caused by the presence of the rich functional groups at GO nanosheets [57], such as −COOH, −OH, and C—O. In addition, it is found that the NiR enzyme functionalization onto the PEDOT NFs-GO reduced the redox current.

CV responses of the sensors with different electrodes were measured at different scan rates (10–100 mV/s). The detailed response curves are given in Fig. S8 (Supplementary information). With increasing scan rate, the peak-to-peak separation voltages for these electrodes shifted toward higher potentials. Because the anodic and cathodic peak currents were shown proportional and inversely proportional with the square root of scan rate, respectively (Fig. 5b), all these electrodes exhibited a surface-controlled process.

A maximum surface concentration of redox couple was obtained for the PEDOT NFs electrode. The high aspect ratio of the PEDOT NFs provided a higher diffusion coefficient, due to delocalized π-electron cloud overlaps in thiophene moiety and long-axis electron transportation with fibers. The surface concentration and diffu-

Table 1
Electrochemical parameters of various fabricated electrodes.

Electrodes	Peak Current I_p (mA)	Peak-to-peak separation voltage ΔE (V)	Surface concentration Γ (mol/cm^2)	Diffusion coefficient D (cm^2/s)	Electro-chemical Area A_{el} (cm^2)	Heterogeneous electron rate k_s (cms^{-1})
Au	0.312	0.345	5.3×10^{-10}	52.03×10^{-7}	0.144	1.05×10^{-4}
PEDOT NFs	1.13	0.275	4.6×10^{-11}	68.25×10^{-6}	0.264	7.5×10^{-4}
PEDOT NFs-GO	0.704	0.172	2.33×10^{-11}	26.49×10^{-6}	0.273	12.4×10^{-4}
NiR/PEDOT NFs-GO	0.429	0.128	1.45×10^{-11}	98.37×10^{-7}	0.280	12.0×10^{-4}

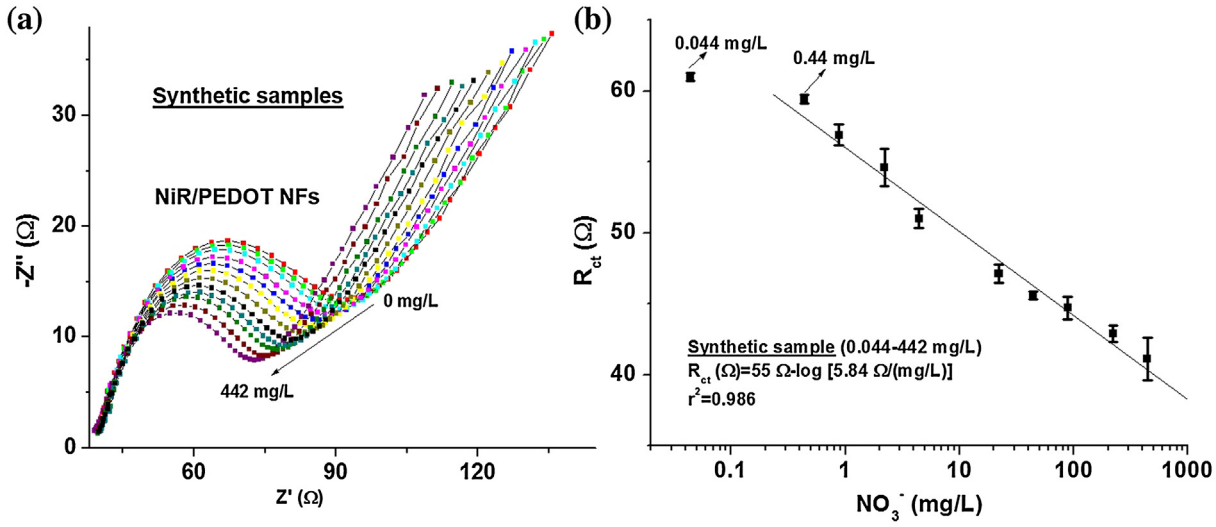

Fig. 6. (a) Electrochemical impedance responses of the fabricated NiR/PEDOT NFs bioelectrode as a function of nitrate ions. (b) R_{ct} of the sensor as a function of nitrate concentration for NiR/PEDOT NFs bioelectrode. Error bars are obtained from three repeated measurements.

sion coefficient consistently decreased, due to the loading of GO nanosheets and protein molecules. The incorporation of GO sheets into the NFs also enhanced the effective electrochemical area. A maximum k_s value was obtained on the PEDOT NFs-GO electrode, compared to the other electrodes (Table 1). This is presumably due to the highly anisotropic tunneling conduction of electrons associated with the 1D feature of the polymer along the chains when intercalating with the benzoid structure of GO. The use of PEDOT NFs-GO enabled a larger electrochemical surface area and a higher heterogeneous electron transfer rate than the use of PEDOT NFs only, leading to an improved sensor efficacy. While the enzyme functionalization on the PEDOT NFs-GO resulted in a decrease in the ion diffusion coefficient of the electrode, the high values of k_s, D and A_{el} demonstrated that the NiR/PEDOT NFs-GO composite integrated in the sensor acted as a suitable bioelectrode.

EIS method was used to measure the impedance of the electrode/electrolyte interface by applying a sinusoidal AC potential to the electrochemical cell. Fig. 5c and d show the EIS spectra for the fabricated sensors. A low R_{ct} value of 15.5 Ω was obtained at the PEDOT NFs. The GO incorporation led to an increased value of R_{ct} to 35.6 Ω. After the enzyme immobilization, the PEDOT NFs electrodes with and without GO provided increased values of R_{ct} due to the insulating nature of enzyme molecules on its surface. Among all the fabricated electrodes, the PEDOT NFs-GO electrode showed the highest value of R_{ct} at 126 Ω. Table S4 shows the electrochemical parameters, including R_{ct}, C_{dl}, and time constant τ obtained from the EIS spectra in Fig. 5c and d and Eqs. S10–S14 (Supplementary information). After the enzyme immobilization, the value of τ for the NiR/PEDOT NFs-GO electrode became higher than that for the NiR/PEDOT NFs (Table S4 in Supplementary information), because of the slow diffusion of $[Fe(CN)_6]^{3-/4-}$ ions at the electrode enzyme layer/solution interface.

3.4. Detection of nitrate ions

We first evaluated the ability of the microfluidic sensor to detect and quantify nitrate ions using the NiR/PEDOT NFs based bioelectrode (without GO nanosheets). The EIS measurement method was employed with the sensor. Synthetic solutions with different nitrate concentrations were used. A stock solution of KNO_3 (1000 mg/L) was prepared in de-ionized water and diluted into various concentrations from 0.044 mg/L to 442 mg/L of NO_3^-. Fig. 6a shows the Nyquist plots obtained by the EIS measurements. With increasing nitrate concentration, the value of R_{ct} decreased. Essentially, the nitrate ions at the surface of the electrode reduced to nitrite ions to produce electrons, thus reducing R_{ct}. Fig. 6b shows the calibration plot for R_{ct} as a function of nitrate concentration. As the nitrate concentration increased from 0.044 to 0.44 mg/L, the value of R_{ct} did not significantly reduced, but it did afterwards in the higher concentration range. The sensitivity of the sensor with the NiR/PEDOT NFs-based bioelectrode was calculated as 24.35 Ω/(mg/L)/cm^2 within a wide nitrate concentration range from 0.44–442 mg/L. The LOD of the sensor was calculated using the $3\sigma_b/m$ criteria, where σ_b and m are the standard deviation and slope of the calibration curve [57]. Using the NiR/PEDOT NFs, the sensor was shown to provide a low LOD of 0.68 mg/L or ppm for detecting nitrate ions.

Next, to demonstrate the efficacy of GO nanosheets on the NiR/PEDOT NFs, we conducted EIS measurements for this sensor with GO nanosheets. Fig. 7a and b show the EIS spectra for the sensor responding to different nitrate concentrations of both the synthetic (0.044–442 mg/L) and extracted soil solutions (0.044–44.2 mg/L). Fig. 7c show that the value of R_{ct} decreased with increasing nitrate concentration. The response curve of the sensor for the real samples well overlapped that for the synthetic samples. The relative standard deviation (RSD) for six repeated EIS measurements was as low as 2.9% and 3% for the synthetic and real samples, respectively. This microfluidic sensor exhibited a higher sensitivity of 61.15 Ω/(mg/L)/cm^2 in a range of nitrate concentration from 0.44 to 442 mg/L for the soil solution samples, compared to that using the NiR/PEDOT NFs (24.35 Ω/(mg/L)/cm^2).

In addition, a low LOD of 0.135 mg/L was obtained by this sensor using PEDOT NFs-GO, comparable to that using PEDOT NFs alone (0.68 mg/L). The PEDOT NFs-GO composite provided a larger electrochemical surface area and a higher charge transfer resistance for redox conversions as summarized in Table 1. The rich −COOH, −CHO groups present in this composite allowed sufficient attachment of NiR enzyme molecules to the electrode surface, facilitating more catalytic conversion of nitrate to nitrite ions and thus generating more electrons and larger impedance changes when responding to variations in nitrate concentration. Fig. 7d shows the transient response of this sensor to the presence of nitrate ions at the concentration of 8.82 mg/L. Table 2 compares the performances between our sensors and other typical existing nitrate sensors.

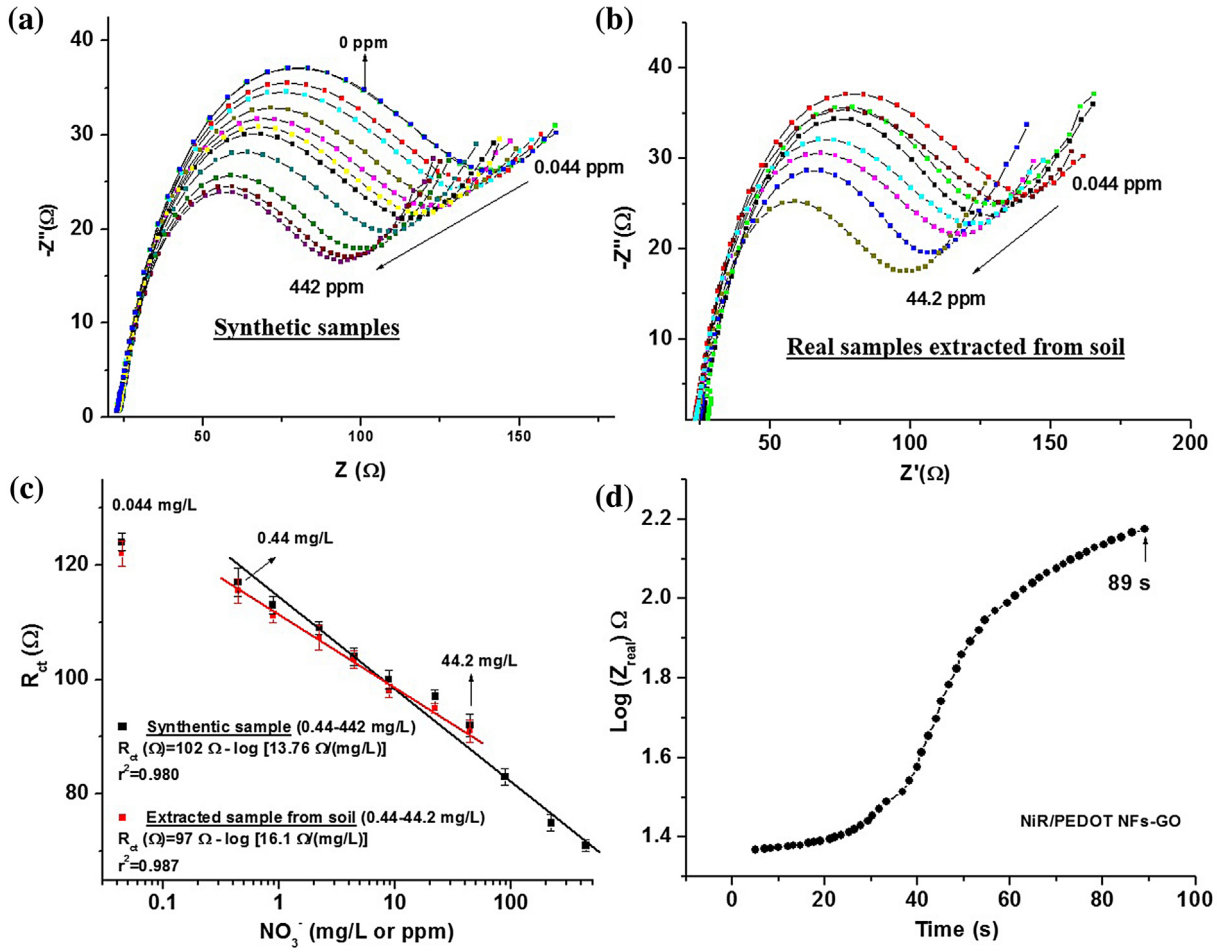

Fig. 7. (a, b) EIS spectra for NiR/PEDOT NFs-GO bioelectrode as a function of nitrate concentration of synthetic samples, and real sample extracted from soil, respectively. (c) R_{ct} of the sensor as a function of concentration of nitrate ions for both synthetic and real samples. (d) Transient response of the sensor to the presence of nitrate ions at the given concentration of 8.82 mg/L.

Table 2
Performance comparison between our sensors and other typical existing nitrate sensors.

Bioelectrode Materials	Measurement Methods	Nitrate Con. Range	Sensitivity	Ref.
Reduced GO	Amperometry	8.9–167 μM	27 nA/μM/cm^2	[4]
1-methyl-3-(pyrrol-1-ylmethyl) pyridinium	Amperometry	100 μM	78 nA/μM/cm^2	[5]
Periplasmic NiR	UV–vis absorption	1.5 μM	NA	[6]
Methyl viologen/Nafion	Conductance	20–250 μM	NA	[7]
CNT/Polypyrrole/NiR	Amperometry	440–1450 μM	0.3 nA/μM/cm^2	[58]
NiR/Polypyrrole	Potentiometric	50–5000 μM	NA	[59]
NiR/PEDOT NFs	Impedance	0.44–442 mg/L or 7.09–7128 μM	24.35 Ω/(mg/L)/cm^2 or 1.51 Ω/μM/cm^2	This work
NiR/PEDOT NFs-GO	Impedance	0.44–442 mg/L or 7.09–7128 μM	61.15 Ω/(mg/L)/cm^{2}or 3.8 Ω/μM/cm^2	This work

3.5. Selectivity, stability and reproducibility studies

To test selectivity of the sensor, we conducted EIS measurements with a fixed concentration of nitrate ions at 44.2 mg/L (synthetic sample) in presence of various interfering ions (Fig. 8a and Fig. S9a and b, Supplementary information). As it is almost impossible to test the sensor with all possible interfering ions, only a few sample ions were tested to demonstrate selectivity of the sensor, including sulfate (SO_4^{2-}; 50 μM concentration), potassium (K^+; 1.06 M), chloride (Cl^-; 0.94 M), and bicarbonate (HCO_3^-; 100 μM). These ions were chosen in the selectivity test because they are important anions and cations in agricultural soil. Because of the immobilized NiR enzyme molecules, the sensor was shown highly specific to nitrate ions even in the presence of the high concentration interfering ions. Specifically, the sensor using the NiR/PEDOT NFs-GO and NiR/PEDOT NFs bioelectrodes exhibited very minute changes in R_{ct} with the interfering ions, as evident by their low RSD values of ±1.51% and ±2.15%, respectively. In case of chloride, the sensor with the NiR/PEDOT NFs-GO bioelectrode exhibited a deviation of 4% from the initial value of R_{ct}, compared to other ions tested. For the sensor using the NiR/PEDOT NFs bioelectrode, a maximum deviation of ±3.2% from the initial value was observed with HCO_3^- ions.

The stability of the sensors with the NiR/PEDOT NFs-GO and NiR/PEDOT NFs bioelectrodes was evaluated by EIS measurements at a regular interval over 24 days (Fig. S9c–d, Supplementary information). Fig. 8b shows the impedance responses of the sensors in the presence of nitrate ions (44.2 mg/L) at a 3-day interval. The sensors were stable during the course of measurement and exhibited only minute deviation from the initial responses. For the sensors

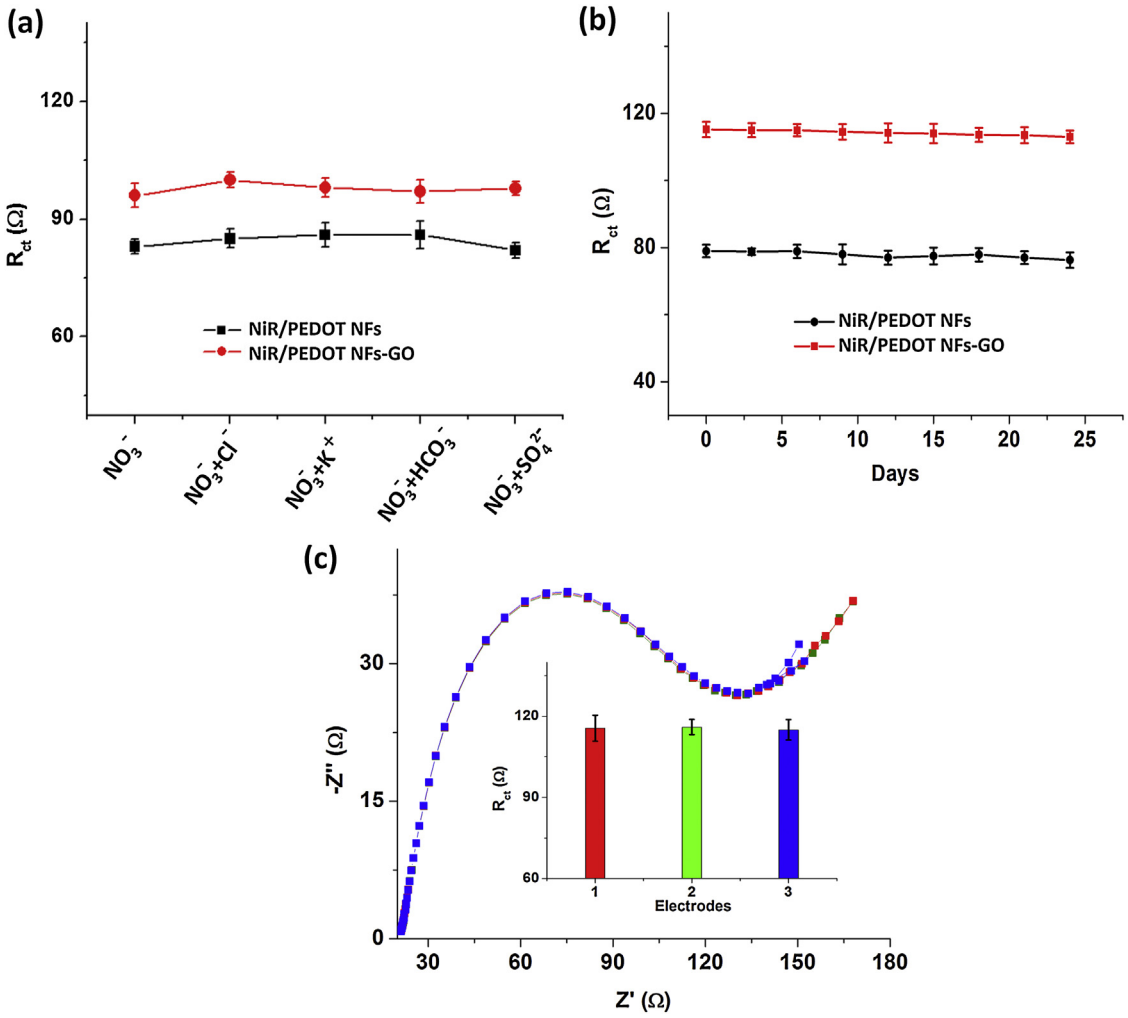

Fig. 8. (a) R_{ct} of the NiR/PEDOT NFs-GO and NiR/PEDOT NFs bioelectrodes in the presence of various interfering ions. (a) R_{ct} of the NiR/PEDOT NFs-GO and NiR/PEDOT NFs bioelectrodes tested for 24 days. (c) EIS spectra for three NiR/PEDOT NFs-GO based nitrate sensors at 44.2 mg/L nitrate concentration. Inset shows a histogram plot for R_{ct} with respect to the three sensors. Error bars are obtained from five repeated measurements.

with the NiR/PEDOT NFs-GO and NiR/PEDOT NFs bioelectrodes, their RSD values were found to be ±2.1% and ±4.0%, respectively, from the corresponding initial responses. We note that the results of the stability test through eight repeatable measurements over 24 days also reflected the reusability of our sensors.

To test the reproducibility of the sensor, we made three identical sensors, with each using the NiR/PEDOT NFs-GO composite as the bioelectrode material. Under the same condition these sensors were used to detect nitrate ions of a given concentration (44.2 mg/L) using the EIS method. Fig. 8c shows the EIS spectra of the sensors, where the inset gives a histogram plot for R_{ct} with respect to different sensors tested. Each sensor ran five repeated EIS measurements. The low RSD of R_{ct} (±1%) from the initial signal indicates that the sensor offered good reproducibility.

4. Conclusions

We demonstrated the microfluidic impedimetric sensor for specific detection of nitrate concentrations in the real samples extracted from soil. The sensor integrated the porous PEDOT NFs-GO composite at its WE material and employed the EIS method to quantify nitrate ion concentrations. The covalent interaction between the PEDOT NFs-GO composite and Au surface by S-Au bonding facilitated easy surface modification of the WE. The NiR enzyme molecules immobilized onto the surface of the PEDOT NFs-GO composite allowed specific detection of nitrate ions even in the presence of other interfering ions in agricultural soils. The abundant functional groups at GO contributed to the strong covalent conjugation with the NiR enzyme molecules resulting in an increased value of R_{ct}. Due to the large electrochemical surface area of the PEDOT NFs-GO composite, the loading capability for the NiR enzyme of the WE increased, thus increasing the dyanmic detection concentration range of the sensor. The GO incorporation allowed enhancing the sensitivity over a test range of 0.044–442 mg/L nitrate ions. The sensor exhibited good selectivity, stability and reproducibility. Efforts are being made to use this microfluidic device for detection of multiple ions by making an array of electrodes with specific recognition molecules.

Acknowledgements

This work is supported in part by the Iowa State University's Plant Sciences Institute, the Iowa Corn Promotion Board, the U.S. National Science Foundation under grants DBI-1353819, CCF-1331390, IIP-1602089 and DGE-1545453, the ISU's Regents Innovation Fund, and the United State Department of Agriculture under grant 2013-68004-20374.

Appendix A. Supplementary data

Supplementary data associated with this article can be found, in the online version, at http://dx.doi.org/10.1016/j.snb.2016.09.101.

References

[1] R.W. Jones, S.J. Rathke, D.A. Laird, J.F. McClelland, Real-time sensing of soil nitrate concentration in the parts per million range while the soil is in motion, Appl. Spectrosc. 67 (2013) 1106–1110.
[2] J.A. Silva, C.I. Evensen, R.L. Bowen, R. Kirby, G.Y. Tsuji, R.S. Yost, Managing Fertilizer Nutrients to Protect the Environment and Human Health, Plant Nutrient Management in Hawaii's Soils, University of Hawaii at Manoa: College of Tropical Agriculture and Human Resources, Manoa, 2000, pp. 7–22.
[3] M.A. Ali, H. Hong, S. Oren, Q. Wang, Y. Wang, H. Jiang, L. Dong, Tunable bioelectrodes with wrinkled-ridged graphene oxide surfaces for electrochemical nitrate sensors, RSC Adv. 6 (2016) 67184–67195.
[4] V. Mani, A.P. Periasamy, S.-M. Chen, Highly selective amperometric nitrite sensor based on chemically reduced graphene oxide modified electrode, Electrochem. Commun. 17 (2012) 75–78.
[5] L.M. Moretto, P. Ugo, M. Zanata, P. Guerriero, C.R. Martin, Nitrate biosensor based on the ultrathin-film composite membrane concept, Anal. Chem. 70 (1998) 2163–2166.
[6] J.W. Aylott, D.J. Richardson, D.A. Russell, Optical biosensing of nitrate ions using a sol-gel immobilized nitrate reductase, Analyst 122 (1997) 77–80.
[7] X.J. Wang, S.V. Dzyadevych, J.M. Chovelon, N.J. Renault, L. Chen, S.Q. Xia, J.F. Zhao, Development of a conductometric nitrate biosensor based on methyl viologen/nafion® composite film, Electrochem. Commun. 8 (2006) 201–205.
[8] A.A. Gokhale, J. Lu, R.R. Weerasiri, J. Yu, I. Lee, Amperometric detection and quantification of nitrate ions using a highly sensitive nanostructured membrane electrocodeposited biosensor array, Electroanalysis 27 (2015) 1127–1137.
[9] N.J. Ronkainen, H.B. Halsall, W.R. Heineman, Electrochemical biosensors, Chem. Soc. Rev. 39 (2010) 1747–1763.
[10] Md. A. Ali, S. Srivastava, K. Mondal, P.M. Chavhan, V.V. Agrawal, R. John, A. Sharma, B.D. Malhotra, A surface functionalized nanoporous titania integrated microfluidic biochip, Nanoscale 6 (2014) 13958–13969.
[11] H. Chang, Y. Yuan, N. Shi, Y. Guan, Electrochemical DNA biosensor based on conducting polyaniline nanotube array, Anal. Chem. 79 (2007) 5111–5115.
[12] H. Peng, L. Zhang, J. Spires, C. Soeller, J. Travas-Sejdic, Synthesis of a functionalized polythiophene as an active substrate for a label-free electrochemical genosensor, Polymer 48 (2007) 3413–3419.
[13] X.Y. Wang, Y.G. Kim, C. Drew, B.C. Ku, J. Kumar, L.A. Samuelson, Electrostatic assembly of conjugated polymer thin layers on electrospun nanofibrous membranes for biosensors, Nano Lett. 4 (2004) 331–334.
[14] K. Markušová, Determination of nitrate in natural waters by voltammetry at a stationary mercury drop electrode, Anal. Chim. Acta 221 (1989) 131–138.
[15] C. Neuhold, K. Kalcher, W. Diewald, X.H. Cai, G. Raber, Voltammetric determination of nitrate with a modified carbon paste electrode, Electroanalysis 6 (1994) 227–236.
[16] L. Ma, B.Y. Zhang, H.L. Li, J.Q. Chambers, Kinetics of nitrate reduction by cobalt-cyclam incorporated nafion® redox polymer, J. Electroanal. Chem. 362 (1993) 201–205.
[17] P. Ugo, L.M. Moretto, B. Ballarin, Nitrate detection at nafion-modified electrodes incorporating ytterbium and uranyl electrocatalysts, Electroanalysis 7 (1995) 129–131.
[18] C.M. Welch, M.E. Hyde, C.E. Banks, R.G. Compton, The detection of nitrate using in-situ copper nanoparticle deposition at a boron doped diamond electrode, Anal. Sci. 21 (2005) 1421–1430.
[19] B. Hafezi, M.R. Majidi, A sensitive and fast electrochemical sensor based on copper nanostructures for nitrate determination in foodstuffs and mineral waters, Anal. Methods. 5 (2013) 3552–3556.
[20] H.D. Tran, D. Li, R.B. Kaner, One-dimensional conducting polymer nanostructures: bulk synthesis and applications, Adv. Mater. 21 (2009) 487–499.
[21] L. Xia, Z. Wei, M. Wan, Conducting polymer nanostructures and their application in biosensors, J. Colloid Interface Sci. 341 (2010) 1–11.
[22] J.A. Arter, D.K. Taggart, T.M. McIntire, R.M. Penner, G.A. Weiss, Virus-PEDOT nanowires for biosensing, Nano Lett. 10 (2010) 4858–4862.
[23] G. Yang, K.L. Kampstra, M.R. Abidian, High performance conducting polymer nanofiber biosensors for detection of biomolecules, Adv. Mater. 26 (2014) 4954–4960.
[24] H. Zhou, W. Yao, G. Li, J. Wang, Y. Lu, Graphene/poly (3, 4-ethylenedioxythiophene) hydrogel with excellent mechanical performance and high conductivity, Carbon 59 (2013) 495–502.
[25] S.M. Richardson-Burns, J.L. Hendricks, B. Foster, L.K. Povlich, D.-H. Kim, D.C. Martin, Polymerization of the conducting polymer poly (3, 4-ethylenedioxythiophene) (PEDOT) around living neural cells, Biomaterials 28 (2007) 1539–1552.
[26] C.M. Hangarter, M. Bangar, A. Mulchandani, N.V. Myung, Conducting polymer nanowires for chemiresistive and fet-based bio/chemical sensors, J. Mater. Chem. 20 (2010) 3131–3140.
[27] A. Kros, R.J.M. Nolte, N. Sommerdijk, Conducting polymers with confined dimensions: track-etch membranes for amperometric biosensor applications, Adv. Mater. 14 (2002) 1779–1782.
[28] A. Wisitsoraat, S. Pakapongpan, C. Sriprachuabwong, D. Phokharatkul, P. Sritongkham, T. Lomas, A. Tuantranont, Graphene-PEDOT:PSS on screen printed carbon electrode for enzymatic biosensing, J. Electroanal. Chem. 704 (2013) 208–213.
[29] C.-Y. Chu, J.-T. Tsai, C.-L. Sun, Synthesis of PEDOT-modified graphene composite materials as flexible electrodes for energy storage and conversion applications, Int. J. Hydrogen Energy 37 (2012) 13880–13886.
[30] T.Y. Huang, C.W. Kung, H.Y. Wei, K.M. Boopathi, C.W. Chu, K.C. Ho, A high performance electrochemical sensor for acetaminophen based on a rGO-PEDOT nanotube composite modified electrode, J. Mater. Chem. A 2 (2014) 7229–7237.
[31] L.M. Lu, O. Zhang, J.K. Xu, Y.P. Wen, X.M. Duan, H.M. Yu, L.P. Wu, T. Nie, A facile one-step redox route for the synthesis of graphene/poly (3,4-ethylenedioxythiophene) nanocomposite and their applications in biosensing, Sens. Actuators B 181 (2013) 567–574.
[32] D.Y. Lee, S.I. Na, S.S. Kim, Graphene oxide/PEDOT: PSS composite hole transport layer for efficient and stable planar heterojunction perovskite solar cells, Nanoscale 8 (2016) 1513–1522.
[33] S. Lehtimäki, M. Suominen, P. Damlin, S. Tuukkanen, C. Kvarnstrom, D. Lupo, Preparation of supercapacitors on flexible substrates with electrodeposited PEDOT/graphene composites, ACS Appl. Mater. Interfaces 7 (2015) 22137–22147.
[34] D. Yoo, J. Kim, J.H. Kim, Direct synthesis of highly conductive poly (3, 4-ethylenedioxythiophene): poly (4-styrenesulfonate)(PEDOT: PSS)/graphene composites and their applications in energy harvesting systems, Nano Res. 7 (2014) 717–730.
[35] M. Zhang, W. Yuan, B. Yao, C. Li, G. Shi, Solution-processed pedot: pss/graphene composites as the electrocatalyst for oxygen reduction reaction, ACS Appl. Mater. Interfaces 6 (2014) 3587–3593.
[36] N. Hui, W. Wang, G. Xu, X. Luo, Graphene oxide doped poly (3, 4-ethylenedioxythiophene) modified with copper nanoparticles for high performance nonenzymatic sensing of glucose, J. Mater. Chem. B 3 (2015) 556–561.
[37] J. Xu, R. Peng, Q. Ran, Y. Xian, Y. Tian, L. Jin, A highly soluble poly (3, 4-ethylenedioxythiophene)-poly (styrene sulfonic acid)/Au nanocomposite for horseradish peroxidase immobilization and biosensing, Talanta 82 (2010) 1511–1515.
[38] Y. Xia, H. Zhang, J. Ouyang, Highly conductive PEDOT: PSS films prepared through a treatment with zwitterions and their application in polymer photovoltaic cells, J. Mater. Chem. 20 (2010) 9740–9747.
[39] P. Santhosh, K.M. Manesh, S. Uthayakumar, S. Komathi, A.I. Gopalan, K.P. Lee, Fabrication of enzymatic glucose biosensor based on palladium nanoparticles dispersed onto poly (3, 4-ethylenedioxythiophene) nanofibers, Bioelectrochemistry 75 (2009) 61–66.
[40] Y. Yang, X. Yang, W. Yang, S. Li, J. Xu, Y. Jiang, Porous conducting polymer and reduced graphene oxide nanocomposites for room temperature gas detection, RSC Adv. 4 (2014) 42546–42553.
[41] J. Zhang, F. Zhang, H. Yang, X. Huang, H. Liu, J. Zhang, S. Guo, Graphene oxide as a matrix for enzyme immobilization, Langmuir 26 (2010) 6083–6085.
[42] S. Nair, E. Hsiao, S.H. Kim, Melt-welding and improved electrical conductivity of nonwoven porous nanofiber mats of poly (3, 4-ethylenedioxythiophene) grown on electrospun polystyrene fiber template, Chem. Mater. 21 (2008) 115–121.
[43] S.J. Park, H.S. Song, O.S. Kwon, J.H. Chung, S.H. Lee, J.H. An, S.R. Ahn, J.E. Lee, H. Yoon, T.H. Park, J. Jang, Human dopamine receptor nanovesicles for gate-potential modulators in high-performance field-effect transistor biosensors, Sci. Rep. 4 (2014) 4342.
[44] H.-B. Bu, G. Götz, E. Reinold, A. Vogt, S. Schmid, R. Blanco, J.L. Segura, P. Bäuerle, Click-functionalization of conducting poly (3, 4-ethylenedioxythiophene) (PEDOT), Chem. Commun. 11 (2008) 1320–1322.
[45] S.-C. Luo, E.M. Ali, N.C. Tansil, H.-H. Yu, S. Gao, E.A.B. Kantchev, J.Y. Ying, Poly (3, 4-ethylenedioxythiophene) (PEDOT) nanobiointerfaces: thin, ultrasmooth, and functionalized PEDOT films with in vitro and In vivo biocompatibility, Langmuir 24 (2008) 8071–8077.
[46] S.-C. Luo, S.S. Liour, H.-h. Yu, Perfluoro-functionalized PEDOT films with controlled morphology as superhydrophobic coatings and biointerfaces with enhanced cell adhesion, Chem. Commun. 46 (2010) 4731–4733.
[47] A.J. Demello, Control and detection of chemical reactions in microfluidic systems, Nature 442 (2006) 394–402.
[48] M.A. Ali, K.K. Reza, S. Srivastava, V.V. Agrawal, R. John, B.D. Malhotra, Lipid-lipid interactions in aminated reduced graphene oxide interface for biosensing application, Langmuir 30 (2014) 4192–4201.
[49] R. Hood-Nowotny, N. Hinko-Najera Umana, E. Inselbacher, P. Oswald-Lachouani, W. Wanek, Alternative methods for measuring inorganic, organic, and total dissolved nitrogen in soil, Soil Sci. Soc. Am. J. 74 (2010) 1018–1027.
[50] M.A. Rahman, N.-H. Kwon, M.-S. Won, E.S. Choe, Y.-B. Shim, Functionalized conducting polymer as an enzyme-immobilizing substrate: an amperometric glutamate microbiosensor for In Vivo measurements, Anal. Chem. 77 (2005) 4854–4860.
[51] X. Bai, X. Hu, S. Zhou, J. Yan, C. Sun, P. Chen, L. Li, Controlled fabrication of highly conductive three-dimensional flowerlike poly (3,

4-ethylenedioxythiophene) nanostructures, J. Mater. Chem. 21 (2011) 7123–7129.
[52] J. Noh, E. Ito, K. Nakajima, J. Kim, H. Lee, M. Hara, High-resolution STM and XPS studies of thiophene self-assembled monolayers on Au (111), J. Phys. Chem. B 106 (2002) 7139–7141.
[53] J.H. Jung, D.S. Cheon, F. Liu, K.B. Lee, T.S. Seo, A graphene oxide based immuno-biosensor for pathogen detection, Angew. Chem. Int. Ed. 49 (2010) 5708–5711.
[54] C. Chen, T. Zhang, Q. Zhang, Z. Feng, C. Zhu, Y. Yu, K. Li, M. Zhao, J. Yang, J. Liu, D. Sun, Three-dimensional BC/PEDOT composite nanofibers with high performance for electrode-cell Interface, ACS Appl. Mater. Interfaces 7 (2015) 28244–28253.
[55] X. Luo, C.L. Weaver, S. Tan, X.T. Cui, v Pure graphene oxide doped conducting polymer nanocomposite for bio-interfacing, J. Mater. Chem. B 1 (2013) 1340–1348.
[56] D. Du, L. Wang, Y. Shao, J. Wang, M.H. Engelhard, Y. Lin, Functionalized graphene oxide as a nanocarrier in a multienzyme labeling amplification strategy for ultrasensitive electrochemical immunoassay of phosphorylated p53 (S392), Anal. Chem. 83 (2011) 746–752.
[57] S. Srivastava, S. Abraham, C. Singh, Md A. Ali, A. Srivastava, G. Sumana, B.D. Malhotra, Protein conjugated carboxylated gold@ reduced graphene oxide for aflatoxin B 1 detection, RSC Adv. 5 (2015) 5406–5414.
[58] F. Can, S.K. Ozoner, P. Ergenekon, E. Erhan, Amperometric nitrate biosensor based on carbon nanotube/polypyrrole/nitrate reductase biofilm electrode, Mater. Sci. Eng. C 32 (2012) 18–23.
[59] M. Sohail, S.B. Adeloju, Fabrication of redox-mediator supported potentiometric nitrate biosensor with nitrate reductase, Electroanalysis 21 (2009) 1411–1418.

Biographies

Md. Azahar Ali received his Ph.D. degree from the Biomedical Engineering Department at Indian Institute of Technology Hyderabad, India, in collaboration with the Biomedical Instrumentation Section at National Physical Laboratory, New Delhi, India, in 2014. He also received his Master of Technology degree from the Department of Electronics Engineering at Tezpur University, Assam, India, in 2009. Currently, he is a Post-Doctoral Research Associate in the Department of Electrical and Computer Engineering at Iowa State University. He is actively engaged in the area of microfluidic and MEMS sensors in agriculture and biomedicine.

Huawei Jiang received her Ph.D. degree in Electrical Engineering from the Department of Electrical and Computer Engineering at Iowa State University, Ames, Iowa, USA, in 2016. She also received her M.S. degree in Chemical Engineering from the Dalian University of Technology, Dalian, China, in 2010. Currently, she is Post-Doctoral Research Associate in the Laboratory for MEMS and Biochips at Iowa State University. Her research is focused on the development of microfluidic devices for plant phenotyping and microbial fuel cells.

Navreet K. Mahal earned her B.S. degree from the Punjab Agricultural University and M.S. degree in Soil Science from the Fresno State University. Navreet is now a Ph.D. candidate at the Iowa State University. Navreet's research and teaching interests focus on improving nitrogen use efficiency and maximizing sustainable production in cereal crop systems.

Robert J. Weber began his prolific career in the Solid State Research Laboratory at the Collins Radio Company, later a part of Rockwell International. For 25 years, he was involved in advanced development and applied research in the one-to-ten-GHz frequency range and received several distinguished awards for his valuable contributions to this field. He has taught microwave circuit design and fiber-optics communications with the Department of Electrical and Computer Engineering, Iowa State University. He is currently involved in ongoing experimental research in integrating microwave circuits with other devices such as energy harvesters, MEMS, electronic and chemical sensors, and electro-optics.

Ratnesh Kumar is a Professor of electrical and computer engineering with the Iowa State University since 2002. Prior to this, he was on faculty with the University of Kentucky from 1991 to 2002 in electrical and computer engineering, and has held visiting positions with the University of Maryland, the Applied Research Laboratory (at Penn State University), NASA Ames, the Idaho National Laboratory, the United Technologies Research Center, and Air Force Research Laboratory. He received the B. Tech. degree in electrical engineering from IIT Kanpur, India, and the M.S. and Ph.D. degrees in electrical and computer engineering from the University of Texas, Austin, TX, USA, in 1987, 1989, and 1991, respectively. He received the Gold Medals for the Best EE Undergrad and the Best All Rounder from IIT Kanpur, and the Best Dissertation Award from UT Austin. He is a Fellow of the IEEE, a Distinguished Lecturer for the IEEE Control Systems Society, Best Paper Award recipient from IEEE Transactions on Automation Science and Engineering.

Michael J. Castellano is the William T. Frankenberger Professor of Soil Science the Agronomy Department at Iowa State University. He received his PhD in Soil Science in 2009 from The Pennsylvania State University. His research focuses on maximizing sustainable productivity of crop systems. He has particular interest in nitrogen because nitrogen is a costly input and often limits crop production, but is easily lost to the environment where it becomes an economic loss that degrades air and water quality.

Liang Dong is an Associate Professor in the Department of Electrical and Computer Engineering at Iowa State University. He received his Ph.D. degree in Electronic Science and Technology from the Institute of Microelectronics at Tsinghua University, Beijing, China in 2004. From 2004 to 2007, he was a Postdoctoral Research Associate in the Department of Electrical and Computer Engineering at University of Wisconsin-Madison. He has a courtesy appointment at the Iowa State's Department of Chemical and Biological Engineering and is an associate of the U.S. DOE's Ames Laboratory. Dr. Dong is a Faculty Scholar of the Plant Sciences Institute at Iowa State University. He serves as an Editorial Board Member of journal Scientific Reports and a Guest Editor of journal Micromachines. He previously received the National Science Foundation CAREER Award, the Early Career Engineering Faculty Research Award, the Harpole-Pentair Developing Faculty Award, and the Warren B. Boast Undergraduate Teaching Award at Iowa State University. Before coming to the U.S., he received the Top 100 National Outstanding Doctoral Dissertation Award in China, and was one of ten recipients of the Academic Rising Stars in Tsinghua University. His current research interests include MEMS, microfluidics, sensors, nanophotonics and micro/nanomanufacturing, and their applications in sustainable agriculture and environments, plant sciences, biomedicine, and Internet-of-Things devices.